RMetS
Royal Meteorological Society

The essential ingredients leading to the explosive growth stage of the European wind storm *Lothar* of Christmas 1999

G. Rivière[a]*, P. Arbogast[a], K. Maynard[b] and A. Joly[a]
[a]*CNRM/GAME, Météo-France/CNRS, Toulouse, France*
[b]*DPrevi/Labo, Météo-France, Toulouse, France*
*Correspondence to: G. Rivière, Météo-France, CNRM/GMAP/RECYF, 42 av. G. Coriolis, 31057 Toulouse Cedex 1, France. E-mail: gwendal.riviere@meteo.fr

Key dynamical ingredients leading to the explosive growth stage of the extratropical wind storm *Lothar* (24–26 December 1999) are identified by performing numerical sensitivity experiments using the Météo-France operational model. This stage suddenly occurred when the surface cyclone crossed the upper-level jet in its exit region. The model is shown to capture quite well the whole process by starting the forecast 12 h before the start of the explosive growth stage.

A first set of experiments consists of revisiting the role of humidity and other physical processes. A run suppressing latent heating does not exhibit any cyclone growth, similar to a previous study by other authors. However, a frictionless dry adiabatic run, i.e. when latent heating processes and dissipation terms are both suppressed, is shown to reproduce the timing and the location of the rapid intensification stage but not its intensity (which is overestimated). Moist processes are thus crucial because they compensate for the dissipation terms, but the vertical coupling between the surface cyclone and the upper-level jet can be reproduced and interpreted in terms of frictionless dry adiabatic interactions, at least for conceptual purposes.

All the other numerical experiments have the full physics of the model and only differ in their initial conditions. The modification of the flow is performed using a recently developed potential vorticity inversion method. Upper-level high-frequency anomalies are shown to have only a moderate impact on the rapid deepening of the surface cyclone. Other experiments are conducted to look at the sensitivity to the strength of the upper-level jet, to the intensity of the low-level baroclinicity, to the location of the jet exit and finally to the shape, amplitude and location of the low-level cyclone. The location of the explosive growth stage depends primarily on the position of the low-frequency jet exit while its intensity and even its existence is strongly sensitive to the low-level background baroclinicity and to the properties of the incipient surface cyclone itself. Copyright © 2010 Royal Meteorological Society

Key Words: extratropical wind storm; jet exit; PV inversion

Received 12 June 2009; Revised 14 October 2009; Accepted 16 December 2009; Published online in Wiley InterScience

Citation: Rivière G, Arbogast P, Maynard K, Joly A. 2010. The essential ingredients leading to the explosive growth stage of the European wind storm *Lothar* of Christmas 1999. *Q. J. R. Meteorol. Soc.* DOI:10.1002/qj.585

1. Introduction

At the end of December 1999, two successive extreme wind storms, called *Lothar* (24–26 December 1999; hereafter denoted as T1) and *Martin* (26–28 December 1999; hereafter T2) hit western Europe leading to spectacular disasters and many human fatalities. The former storm crossed and affected several countries (France, Germany and Switzerland) while the effects of the latter were more localized in southwestern France. The large-scale environment in which the two storms formed was characterized by a very intense upper-level zonal jet (more

than 80 m s^{-1}) and very strong baroclinicity (Ulbrich *et al.*, 2001). Despite some differences between the two storms which we will address later, the two storms had common features; both were initially formed in the western Atlantic far south of the upper-level jet (almost 10° to the south), were translated across the Atlantic basin with moderate amplitude and were strongly and rapidly deepened as they travelled poleward across the upper-level jet axis more or less at the same time as they reached the French Atlantic coast.

Their trajectory and the location of their explosive growth stage were found to be closely linked with the three-dimensional properties of the large-scale environment by Rivière and Joly (2006, hereafter RJ06). More precisely, the path and the shape of the two low-level cyclones over the Atlantic were related to a low-frequency low-level jet and its deformation field. While this low-frequency low-level jet was far south of the low-frequency upper-level jet over the central Atlantic where the baroclinicity was the strongest, the two jets came closer to each other farther east and were vertically aligned at longitudes 10° W–0° (Figure 3(a) in RJ06). The superposition of these two jets in the eastern Atlantic formed what is called in RJ06 a baroclinic critical region, that is, a specific area where surface cyclones may strongly interact baroclinically with upper-level dynamical features. The baroclinic critical region was located far downstream of the baroclinicity maximum and provided a rationale for the location of the explosive growth stage of the two storms. Such a region was intrinsically related to the formation of an intense upper-level jet and is thus quite rare.

Despite these similarities due to the same large-scale environment in which they were embedded, significant discrepancies between the two storms also existed. A well-defined pre-existing upper-level precursor was found for T2, whereas no such upper-level feature was detected prior to the formation of T1 (Wernli *et al.*, 2002, hereafter W02; Hello and Arbogast, 2004). While the former can be considered as a classical type-B cyclogenesis (Petterssen and Smebye, 1971), it is more difficult to classify the latter as a given type of cyclogenesis. In an attempt to relate T1 to the generalized linear baroclinic instability theory, Descamps *et al.* (2007) have compared the structure of the low-level cyclone with that of the energy singular vectors but found little resemblance between the two. The cyclogenesis theory that seems to match the behaviour of T1 the closest is the concept of 'diabatic Rossby wave' as shown by W02. A shallow and small-scale low-level cyclone translating across the Atlantic with an intense condensational heating continuously regenerating the low-level potential vorticity (PV) anomaly corresponds to a typical feature of a 'diabatic Rossby wave'. Furthermore, W02 have compared two simulations of a high-resolution model, one with moist processes and the other without them, and found that the latter run was not able to capture the intensification stage of T1. Hence, W02 have underlined the key role played by moist processes during the whole life cycle of T1.

Because of the unusual dynamical properties outlined above, the present study is focused on T1 and the key ingredients leading to its explosive growth stage (also called hereafter the rapid intensification stage). Sensitivity numerical experiments are carried out using the Météo-France operational global model. A first set of experiments consists of revisiting diabatic effects. Although moist processes were shown to be essential to explain the intensification stage in the presence of dissipative processes, it is not obvious that a pure adiabatic run (by removing all the sources and sinks) is not able to capture some aspects of the interaction of the low-level cyclone with the upper-level jet. In other words, the question asked is still: are dry dynamics able to reproduce the explosive growth stage of T1?

Another set of numerical experiments is based on the modification of the initial conditions 12 h before the start of the explosive growth stage with the help of the PV-inversion tool of Arbogast *et al.* (2008). Even though the low-level cyclone has formed without the pre-existence of an upper-level precursor, high-frequency disturbances in the upper troposphere were detected before the intensification stage (RJ06) and may play a role during the latter stage. The impact of these upper-level high-frequency anomalies are first analyzed by removing them at the initial time. Other experiments are conducted to explore the sensitivity to the strength of the upper-level jet, to the low-level baroclinicity, and finally to the shape, amplitude and location of the low-level cyclone.

The model and the methodology are presented in section 2. Section 3 investigates the role of humidity and other physical processes. The role of the high-frequency disturbances and of several components of the low-frequency environment are analyzed in sections 4 and 5 respectively. The last set of numerical experiments is presented in section 6 and consists of initializing the model with idealized low-level cyclones having different shapes and locations. A conclusion is provided in section 7.

2. Methodology and control experiment

2.1. Model

The model used is the global primitive-equation forecast model ARPEGE-IFS (Action de Recherches Petite Echelle Grande Echelle–Integrated Forecast System) of Météo-France (Courtier *et al.*, 1991). It has 46 hybrid levels in the vertical and a stretched horizontal grid maximizing resolution over France. The model resolution (30 km on average over the northeastern Atlantic) and the number of vertical levels correspond roughly to the same characteristics as those used in other numerical experiments on T1 (W02; Røsting and Kristjánsson, 2006).

Except in section 3, the full physics of the model are used. Moist processes are parametrized by evolved versions of a mass flux scheme of deep convection (Bougeault, 1985) and of the prognostic large-scale precipitation scheme of Lopez (2002). Other diabatic processes comprise a first-order vertical turbulent diffusion scheme, a shallow convection scheme, a mountain drag parametrization, a radiative transfer scheme (Morcrette *et al.*, 2001) and the land surface scheme ISBA (Noilhan and Planton, 1989).

The model is initialized with the 4D-Var ARPEGE analysis of December 1999. Note that the operational version of the model had a T199 resolution at that time and thus a more recent version is used in the present study with a much higher resolution. All the data

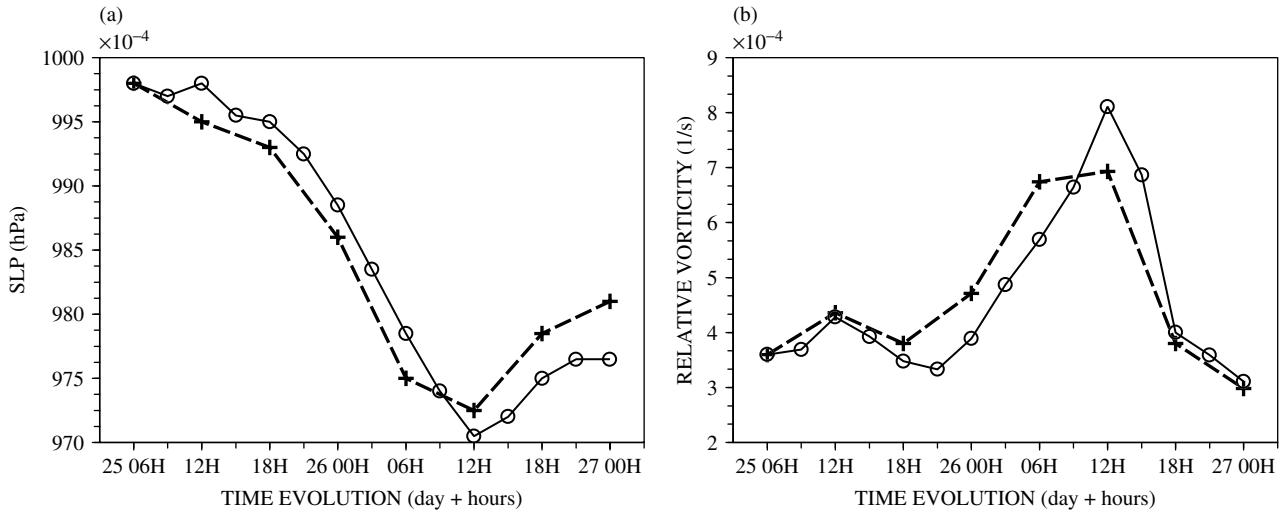

Figure 1. Time evolution of (a) the minimum sea-level pressure and (b) the maximum relative vorticity at 850 hPa over the low-level cyclone for the operational analysis (dashed line with +) and the control forecast (solid line with ○).

of the different numerical experiments are interpolated every 3 h onto a regular longitude/latitude grid with a horizontal resolution of 0.5°. This resolution has been found more appropriate than a 1.5° grid to capture the relative small-scale structure of the low-level cyclone.

2.2. *Operational analysis and control experiment*

The explosive growth stage of T1 is evident in the operational analyses from 1800 UTC, 25 December to 1200 UTC, 26 December with the most rapid deepening occurring between 0000 and 0600 UTC, 26 December (Figure 1). The sea-level pressure (SLP) minimum falls to almost 972.5 hPa at the same time as the relative vorticity maximum reaches its highest value ($6.9 \times 10^{-4}\,s^{-1}$) at 1200 UTC, 26 December. A control forecast (hereafter denoted as CTRL) starting at 0600 UTC on 25 December (i.e. almost 12 h before the start of the intensification stage in the operational analysis) captures very well the timing and the intensity of the explosive growth stage (Figure 1). The latter started at 0000 UTC on 26 December, slightly later than in the operational analysis, and ended at 1200 UTC on 26 December, when the SLP minimum and the relative vorticity maximum reached 970.5 hPa and $8.1 \times 10^{-4}\,s^{-1}$ respectively.

The shape and the trajectory of the surface cyclone as well as the location of its explosive growth stage are very similar in the control forecast and the operational analysis as shown in Figure 2. Between 0600 and 1800 UTC on 25 December, the surface cyclone in both cases moved northeastward at the same speed without any intensification of the relative vorticity but with an increase of the vertical velocity as it came closer to the upper-level jet axis (compare Figure 2(a) with 2(c) and Figure 2(b) with 2(d)). The interaction with upper-level features is also visible at 1800 UTC on 25 December with a strong anticyclonic upper-level circulation northeast of the surface cyclone (Figures 2(c),(d)). At 0600 UTC on 26 December (Figures 2(e),(f)), the surface cyclone was just below a region of positive upper-level relative vorticity and had just crossed the upper-level jet axis. From 0600 to 1200 UTC on 26 December, high values of the low-level relative vorticity are vertically aligned with their equivalent at upper levels, and it is at this time that most of the damage occurred in France, Germany and Switzerland. This later stage is also shown in Figure 3 in terms of upper-level geopotential and SLP. The position and the value of the SLP minimum as well as the scale of the cyclone are well represented in the control forecast. Furthermore, an upper trough is evident in the geopotential field above the SLP minimum at 1200 UTC on 26 December (30 h forecast) and not before, similar to what happens in the operational analysis.

2.3. *The PV-inversion method*

The Ertel PV-inversion algorithm described in Arbogast *et al.* (2008) is applied within the framework of the ARPEGE-IFS system. Instead of solving balance equations, the nonlinear algorithm solves iteratively a variational problem in which the energy of the distance between the iterate and the subspace of the model solutions is minimized. The distance is calculated using a projection of each iterate onto the model subspace with a digital filter initialization approach. This procedure filters out periods less than 3 h. The method provides all the variables from the sole knowledge of the three-dimensional PV and of a Neumann boundary condition which is given by the temperature at 850 hPa.

2.4. *Definition of the anomalies*

Anomalies are built and substracted from the operational analysis to get new initial conditions and to look at their role in the explosive growth stage of T1. A 33-point temporal filter with a Gaussian shape and a cut-off period of 8 d is applied to the 6-hourly dataset of the operational analysis in order to separate the flow into a high- and a low-frequency part. The former corresponds to the synoptic-scale eddies while the latter to the environment in which they are embedded. The anomalies of PV (q') and of temperature at 850 hPa (T'^{850}) are defined as a combination of these two components of

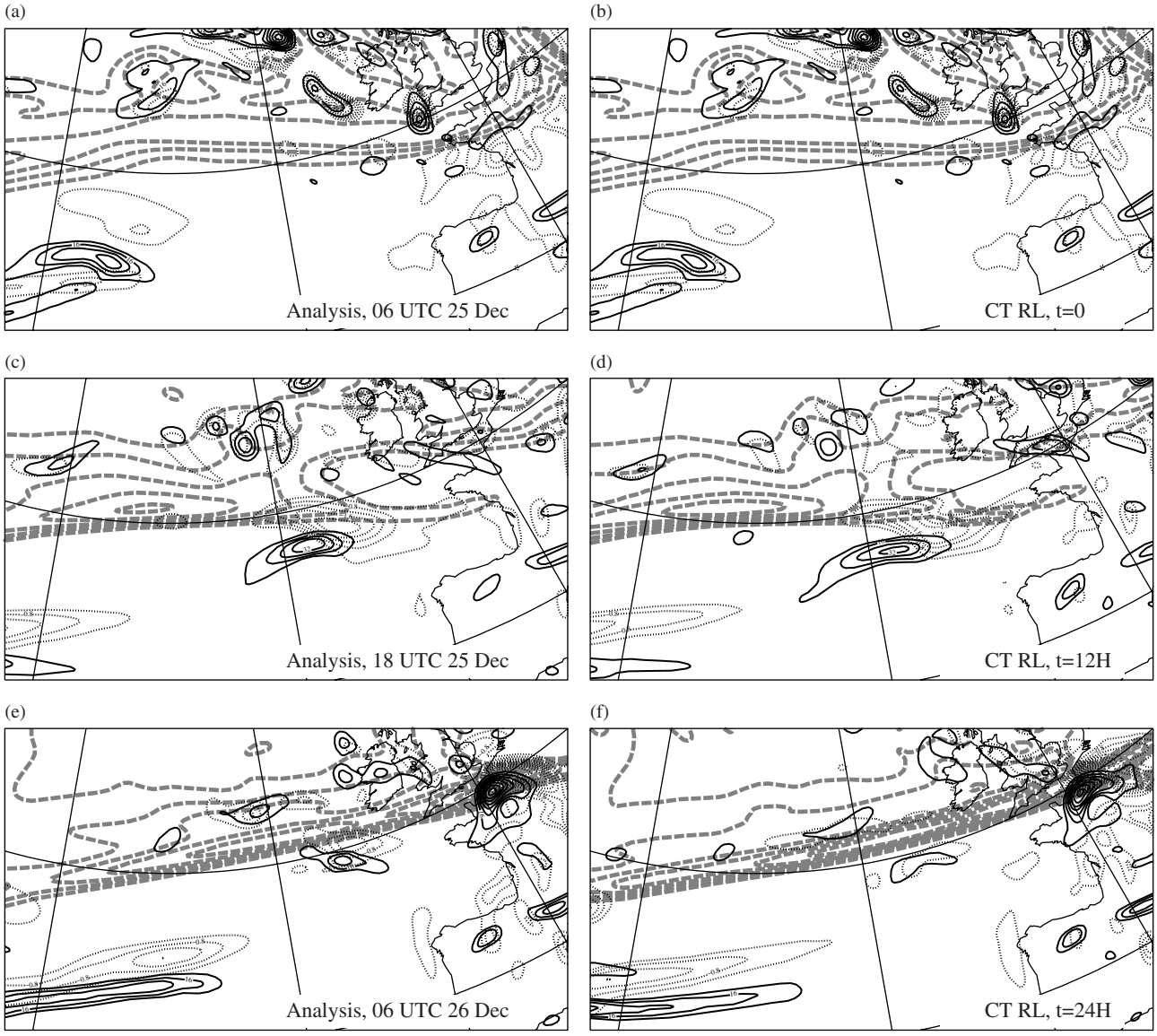

Figure 2. Time evolution of the relative vorticity at 300 hPa (bold dashed grey contours with interval $5 \times 10^{-5}\,\mathrm{s}^{-1}$), and at 850 hPa (black contours with interval $8 \times 10^{-5}\,\mathrm{s}^{-1}$) and the vertical velocity at 600 hPa (dotted contours with interval $0.4\,\mathrm{Pa\,s}^{-1}$ for negative values, i.e. for ascending motions only) for (a, c, e) the operational analysis and (b, d, f) the control forecast ($t = 0, 12, 24$ h): (a, b) 0600 UTC on 25 December, (c, d) 1800 UTC on 25 December, and (e, f) 0600 UTC on 26 December.

the flow as follows:

$$\left.\begin{aligned} q'(x,y,z,t) &= \Big[A_{\mathrm{hf}} q_{\mathrm{hf}}(x,y,z,t) \\ &\quad + A_{\mathrm{lf}}\big\{q_{\mathrm{lf}}(x,y,z,t) - \langle q_{\mathrm{lf}}\rangle(z,t)\big\}\Big] G(x,y), \\ T'^{850}(x,y,t) &= \Big[B_{\mathrm{hf}} T^{850}_{\mathrm{hf}}(x,y,z,t) \\ &\quad + B_{\mathrm{lf}}\big\{T^{850}_{\mathrm{lf}}(x,y,z,t) - \langle T^{850}_{\mathrm{lf}}\rangle(z,t)\big\}\Big] G(x,y), \end{aligned}\right\} \quad (1)$$

where the subscripts $_{\mathrm{hf}}$ and $_{\mathrm{lf}}$ denote the high- and low-frequency parts of the flow respectively. x, y and z denote the horizontal and vertical Cartesian coordinates and $G(x, y)$ is a Gaussian function limiting the spatial extension of the anomaly. A_{hf}, A_{lf}, B_{hf} and B_{lf} are real constant values between 0 and 1. The operator $\langle . \rangle$ denotes a horizontal average over a large domain covering the midlatitude Atlantic basin.

The aim of the decomposition in Eq. (1) is to identify the respective role of each component of the flow in the explosive growth stage of T1. When $A_{\mathrm{lf}} = B_{\mathrm{lf}} = 0$ but A_{hf} and B_{hf} differ from zero, it means that the removed anomaly is composed of synoptic-scale disturbances only. Different sensitivity experiments are then made to the amplitude of the disturbance by modifying the values of A_{hf} and B_{hf}. In contrast, if A_{lf} and B_{lf} differ from zero, the anomaly contains part of the background flow and the numerical experiment is designed to test its impact on T1. However, in order to avoid changing the vertical stratification in that case, the horizontal average $\langle . \rangle$ is applied to the low-frequency part of the anomaly and subtracted from it in Eq. (1).

2.5. *Setting of the sensitivity experiments*

All the sensitivity numerical experiments will start at the same date as the control forecast (0600 UTC, 25 December) by removing some physical processes or some anomalies in the initial condition. The variable which will hereafter be used as a quantitative tool to compare the different

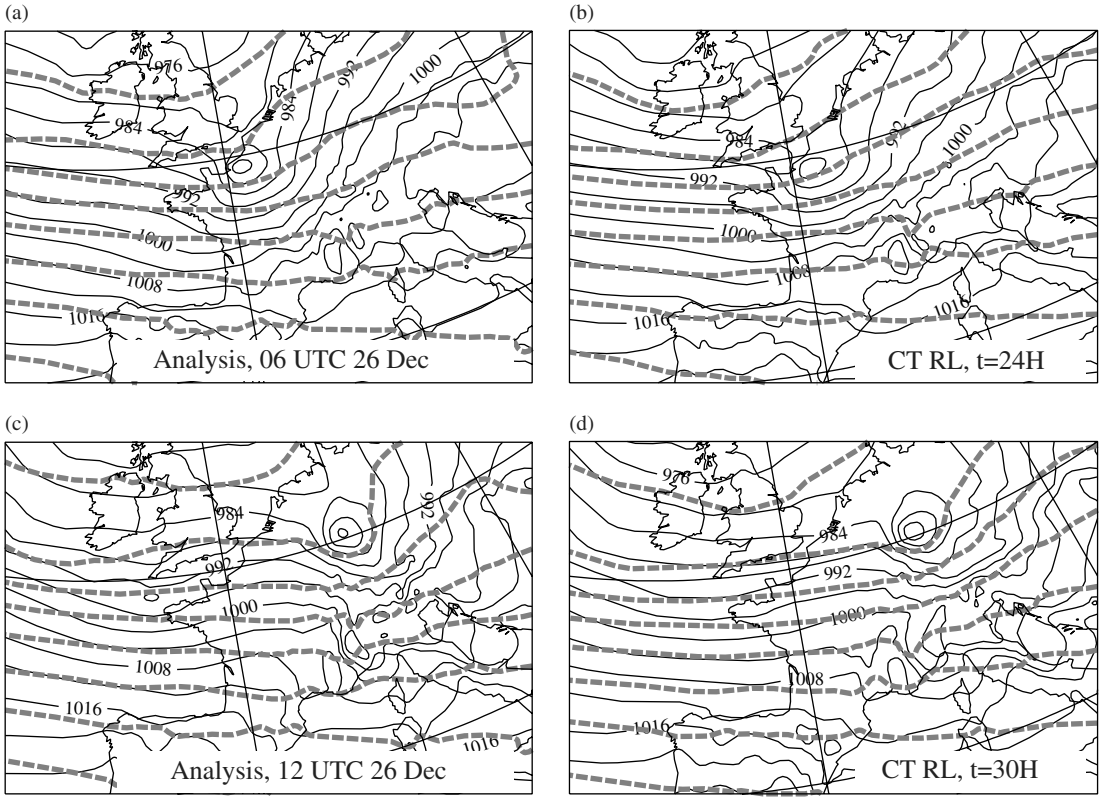

Figure 3. Geopotential at 500 hPa (bold dashed grey contours with interval 1000 $m^2\ s^{-2}$) and sea-level pressure (thin black contours with interval 4 hPa) for (a, c) the operational analysis and (b, d) the control forecast ($t = 24, 30$ h), for (a, b) 0600 UTC on 26 December and (c, d) 1200 UTC on 26 December.

simulations is the relative vorticity maximum at 850 hPa rather than SLP. As shown in Figure 1, there is a continuous decrease of the SLP minimum before 1800 UTC on 25 December which is not due to a deepening of the surface cyclone but rather to its northward displacement and the crossing of the large-scale SLP gradient. The SLP minimum is thus less discriminating than the relative vorticity maximum to detect the explosive growth stage.

3. The role of humidity and other physical processes

In the dry simulation of W02 in which moist processes were suppressed, the surface cyclone was shown to decay without any interaction with upper levels. The authors concluded that moist processes were crucial not only during the incipient phase of T1 and its eastward translation over the Atlantic but also during its intensification stage. The aim of the present section is to revisit the role of physical processes during the latter stage. Moist processes are well known to increase ascending motions and intensify midlatitude cyclones while dissipative processes such as Ekman damping, friction and turbulence have the opposite effects and are sinks of synoptic eddy energy. It is therefore not obvious how the surface cyclone will behave when all these sources and sinks are suppressed in the same run. Otherwise, is a pure adiabatic run able to reproduce the explosive growth stage of T1?

Figure 4 shows that the run without latent heating exhibits a clear decrease of the surface cyclone intensity from the beginning of the simulation, which is consistent with the equivalent simulation of W02. Although its trajectory crosses

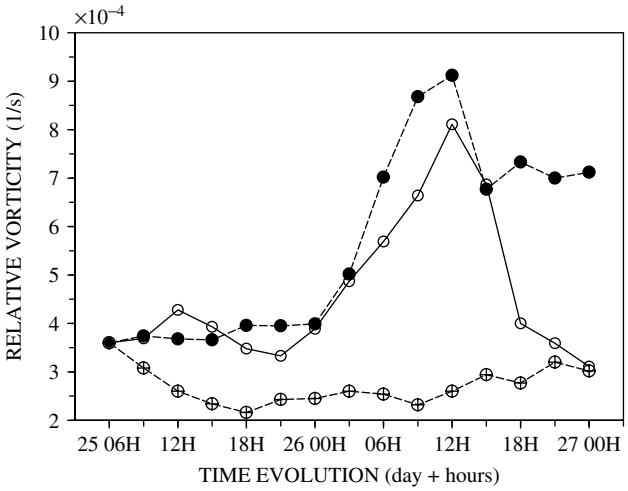

Figure 4. Time evolution of the maximum relative vorticity at 850 hPa for the control run (solid line with ○), the adiabatic run (dashed line with ●) and the run without moist processes (dashed line with ⊕).

the jet axis after 24 h (Figure 5(e)), no deepening of the surface cyclone was detected and no increase of the vertical velocity either. The frictionless adiabatic run (i.e. when the full physics of the model briefly recalled in section 2.1 are suppressed) reproduces quite well the timing and the growth of the intensification stage of the surface cylone (Figures 4 and 5). It keeps a constant amplitude during the first 18 h of the simulation and an abrupt increase of its intensity occurs after that. Note also that its trajectory and the location of its explosive growth stage are similar to CTRL. In particular, it reaches a maximum intensity in northern France and Germany between 0600 and 1200 UTC on 26 December

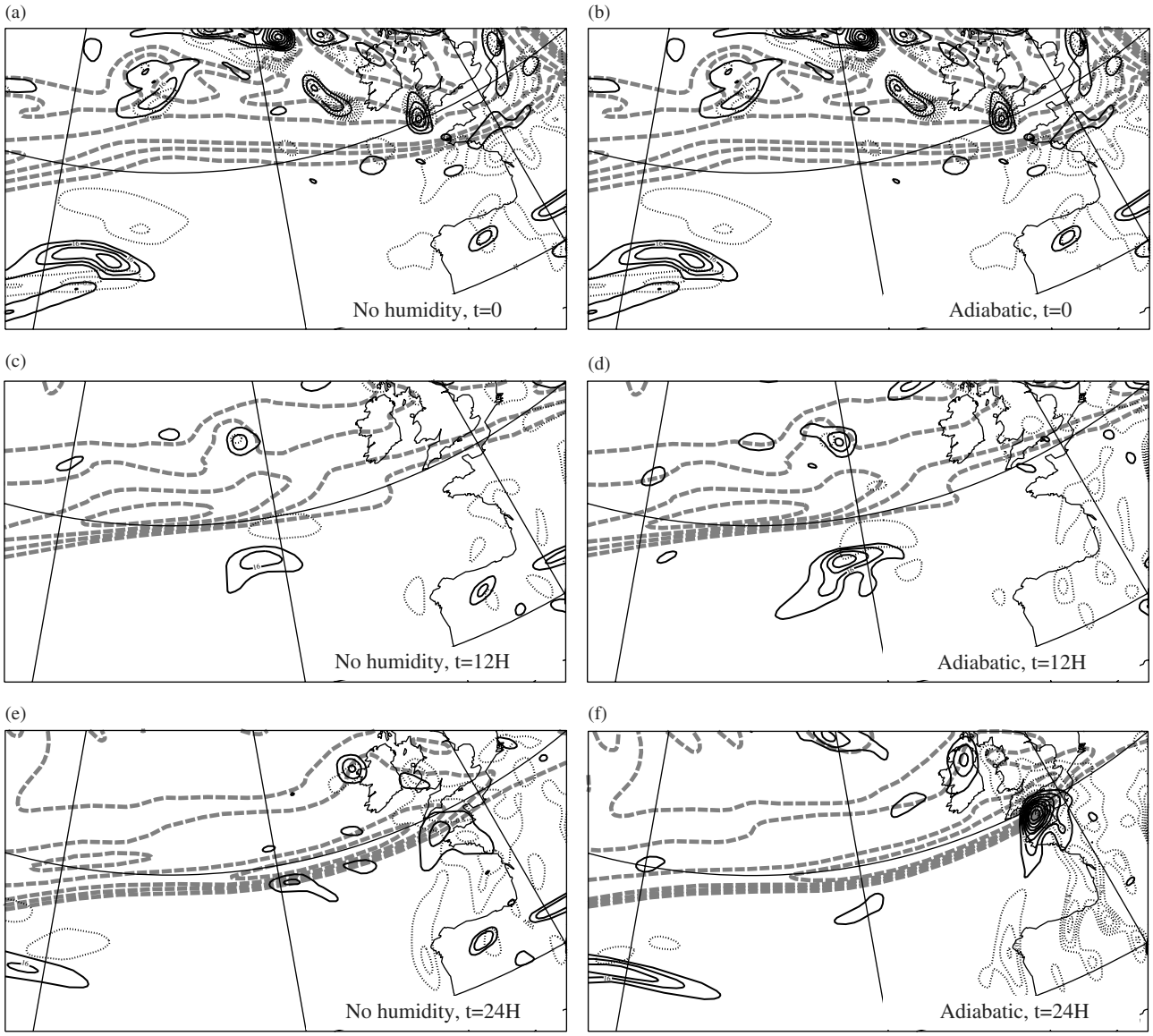

Figure 5. As Figure 2, but for (a, c, e) the run without moist processes and (b, d, f) the adiabatic run.

similar to the storm in CTRL. However, some differences should be underlined. First, the northeastward translation is slightly slower in the adiabatic run; in Figure 5(d) the centre of the surface cyclone is located west of 20° W while in Figure 2(d) it is situated east of that longitude at the same time. This difference is consistent with the well-known increase of the phase speed produced by moist processes; in the presence of full physics, the upward motion to the east of the surface cyclone leads to diabatic heating in that region which increases the eastward propagation of the low-level positive PV (Parker and Thorpe, 1995). Second, the vertical velocity after 12 h did not increase in the adiabatic run whereas it did so at that time in CTRL. The increase of vertical velocity happens later than in CTRL but is evident after 24 h (Figure 5(f)). Note finally that, even though the adiabatic run captures the location and the timing of the explosive growth stage, it is not a realistic scenario in terms of the intensity of the storm since it deepens to almost 940 hPa over the cyclone centre when it reaches western Europe.

To conclude, these experiments show that the amplitude of the surface cyclone is one of the key dynamical parameters in the triggering of the explosive growth stage. In the frictionless adiabatic run, the explosive growth stage occurs because its amplitude is maintained until it reaches the upper-level jet axis since there is no source and sink of energy. In the CTRL run, it is also maintained because sinks and sources compensate one another. Moist processes are thus crucial for the later stage of the real storm because to a large extent they compensate for dissipative effects and maintain the intensity of the surface cylone before its interaction with the upper-level jet. In other words, the role of moist processes is an indirect one, via the maintenance of the low-level vortex. Moist processes may play another role earlier in the formation of the low-level vortex itself, but this aspect is not investigated in the present study since the low-level vortex is already present in our initial conditions. The key fact to retain from the present section is that the interaction of the surface cyclone with the upper-level jet stream during its crossing from the warm to the cold side (as well as the subsequent tropopause fold behind the surface cyclone) can be reproduced and interpreted in the context of dry dynamics. These key steps of the life cycle could therefore be amenable to an understanding expressed only in terms of adiabatic interactions.

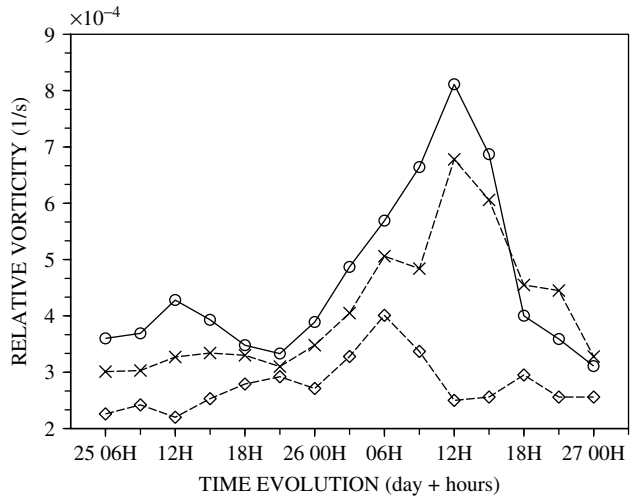

Figure 6. Time evolution of the vorticity maximum at 850 hPa for the control run (solid line with ○), and the runs resulting from removing initially 25% (dashed line with ×) and 50% (dashed line with ◇) of the amplitude of the low-level high-frequency anomalies around T1 between 520 and 850 hPa.

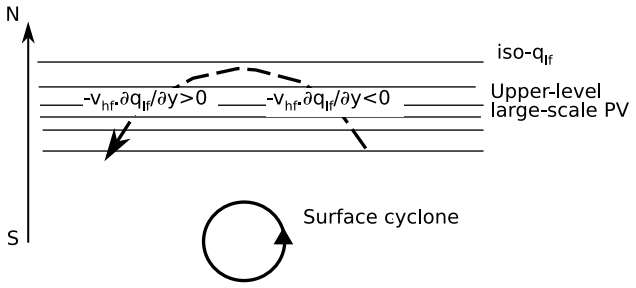

Figure 7. Schematic illustrating how a surface cyclone located south of an upper-level eastward jet may interact with it to create a dipole anomaly in the upper levels. The surface cyclone is represented by the bold solid black line (typically a relative vorticity contour) and the circulation it induces in the upper levels by the dashed black arrow. The large-scale upper-level PV is shown by the zonally oriented thin solid black lines. The advection of the low-frequency upper-level PV by the high-frequency velocity induced by the surface cyclone ($-v_{hf}.\partial q_{lf}/\partial y$) will tend to create a positive PV anomaly to the northwest of the surface cyclone and a negative PV anomaly to the northeast in the upper levels.

4. The role of high-frequency anomalies

4.1. Amplitude of the low-level cyclone

Figure 6 confirms the results of the previous section on the crucial role played by the amplitude of the low-level cyclone but in a different way. The figure depicts the evolution of two runs where the low-level cyclone has initially weaker amplitudes than in CTRL: $A_{hf} = B_{hf}$ are set to 0.25 and 0.50 between 520 and 850 hPa. With a 25% initial amplitude reduction, the explosive growth stage is still present with only a slightly weaker amplitude than in CTRL, while with a 50% amplitude reduction there is almost no significant growth stage. The amplitude of the low-level cyclone is therefore important for its later stage and the sensitivity to the initial amplitude is not linear. There seems to be a threshold value above which rapid growth takes place and leads to a unique result, while below it the growth does not take place.

4.2. High-frequency upper-level anomalies

As already mentioned in the introduction, there is no pre-existing upper-level precursor to T1 and the localized tropopause fold upstream of the low-level cyclone was detected only 6 h before reaching its maximum intensity (W02), i.e. at approximately 0000 UTC on 26 December. However, RJ06 have detected some high-frequency upper-level structures before that time when the surface cyclone was still far south of the upper-level jet. Their possible role in preconditioning the explosive growth stage are investigated in the present section. Assuming an interaction between the upper-level jet and the surface cyclone at 0600 UTC on 25 December (Figure 7), we could expect the formation of a dipole PV anomaly in the upper levels even though they are not close to each other. The high-frequency PV at 300 hPa at 0600 UTC on 25 December (Figure 8(a)) presents negative and positive PV anomalies located northeast and northwest of the surface cyclone respectively, suggesting already an interaction with the upper-level jet at that time. This dipole anomaly is still present at later times with the negative part stronger than the positive one and the node of the dipole is always centred roughly at the same longitude as the surface cyclone (Figures 8(c) and (e)). The vertical structure of the dipole anomaly is shown in Figure 9 and its positive part extends down to 700 hPa.

Is this dipole PV anomaly an important factor that triggers the explosive growth stage? To address this question, the dipole anomaly is removed from the operational analysis using the PV-inversion algorithm. The run without the dipole is shown in Figure 8(b, d, f). The anomaly is built such that $A_{hf} = 1.0$ between 10 and 690 hPa and $A_{lf} = B_{lf} = B_{hf}$ are set to zero. The substraction of the low-frequency PV from the total PV shows no dipole at $t = 0$ (grey contours in Figure 8(b)) but reappears after 12 h (Figure 8(d)) with the node centred at 17° W, 50° N (i.e. few degrees to the north of the low-level relative vorticity maximum). The dipole anomaly intensifies with stronger values on the negative side. There is therefore a regeneration of the dipole anomaly as soon as the simulation starts and the positive values of this dipole become vertically aligned with the surface cyclone after 24 h (Figure 8(f)) when it reaches its maximum intensity (dashed line in Figure 10).

The evolution of the surface cyclone in the run without the initial upper-level dipole anomaly is quite similar to that in CTRL but differs from the latter in a few aspects. Its explosive growth stage is shorter and finishes at $t = 24$ h while in CTRL it happens at $t = 30$ h. Its maximum intensity is reduced by approximately 25% as well. To conclude, the dipole anomaly has a moderate impact on the formation of the storm and is not essential to its explosive growth stage because it is regenerated rapidly through the interaction of the surface cyclone with the strong upper-level large-scale PV gradient. The removal of only the positive part of the dipole anomaly has a weaker impact on the storm development with no more than 5% amplitude reduction compared to CTRL (dotted line in Figure 10). And the run with a suppression of all the high-frequency disturbances in the upper troposphere leads to more or less the same behaviour as in the no dipole case (dash-dotted line in Figure 10) with roughly the same growth rate. As a result, the absence of any upper-level precursor to T1 is confirmed by these experiments. They also show that this important result is compatible with the signatures highlighted by RJ06.

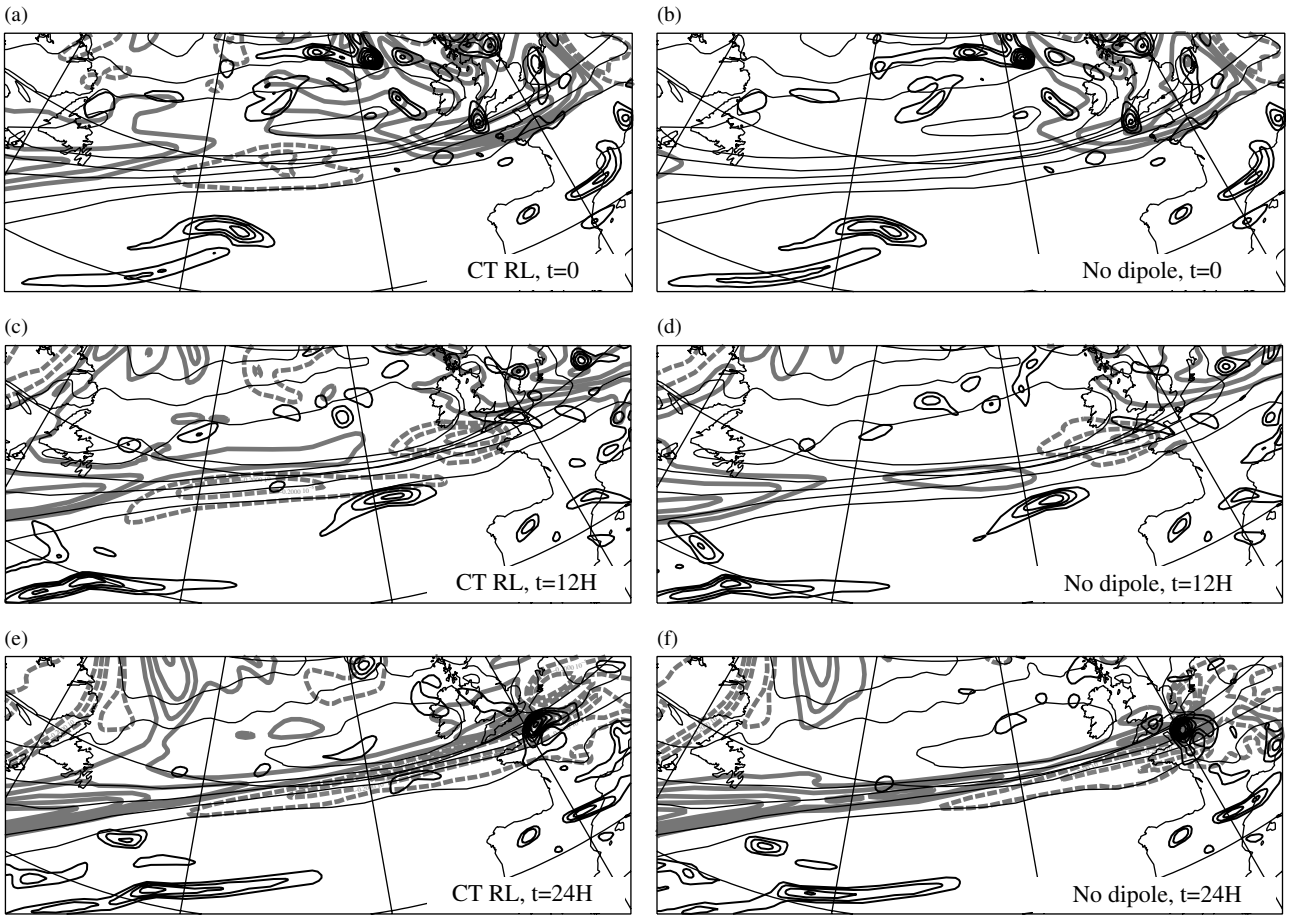

Figure 8. Time evolution ($t = 0, 12, 24$ h) of PV anomalies (PV minus the low-frequency PV of the operational analysis) at 300 hPa (bold dashed and solid grey contours for negative and positive values, with interval 1 PVU $= 10^{-6}\mathrm{m^2 s^{-1} K kg^{-1}}$) and the relative vorticity at 850 hPa (black contours with interval $8 \times 10^{-5}\,\mathrm{s^{-1}}$) for (a, c, e) the control run and (b, d, f) the run initially without the upper-level dipole anomaly. The low-frequency PV of the operational analysis at 300 hPa is shown by thin black contours with interval 1 PVU.

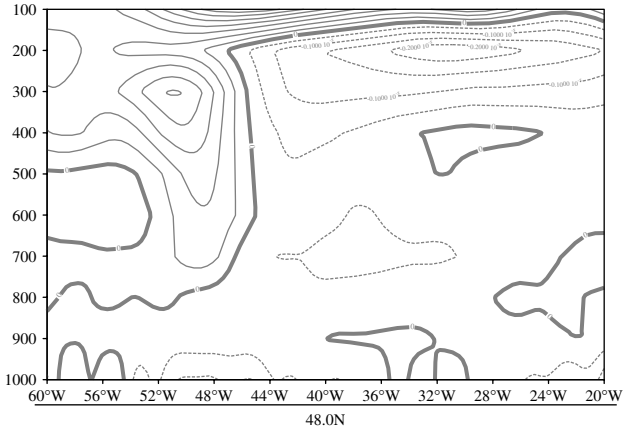

Figure 9. Vertical cross-section at 48° N of the high-frequency PV of the operational analysis. The bold solid contour is zero, the dashed (solid) contours are negative (positive), and the contour interval is 0.5 PVU.

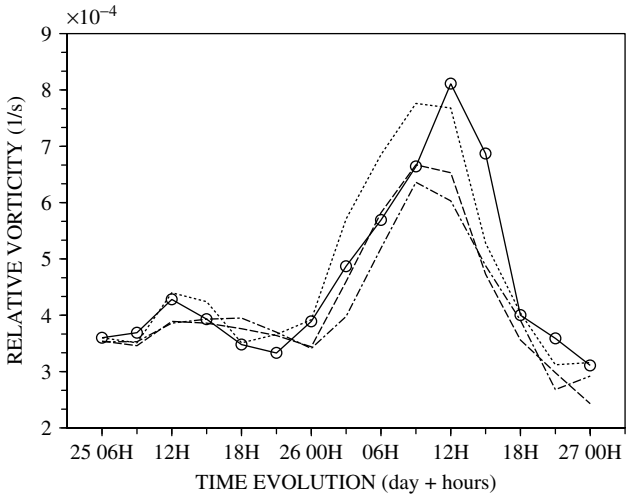

Figure 10. Time evolution of the vorticity maximum at 850 hPa for the control run (solid black line with ○), and the runs without the positive monopole high-frequency PV anomaly (dotted line), without the high-frequency PV anomaly dipole (dashed line), and without the whole high-frequency PV anomalies in the Atlantic domain between 10 and 690 hPa (dash-dotted line).

5. Influence of several components of the low-frequency environment

5.1. Low-frequency disturbances in the whole troposphere

The exceptional strength of the upper-level jet is considered to be one of the key properties of the environment that led to the T1 storm. To quantify its influence, the amplitude of the low-frequency anomalies has been systematically reduced in the whole troposphere. In Figure 11, the upper-level high-frequency signal is altogether removed as in the last experiment above ($A_{\mathrm{hf}} = 1.0$ between 10 and 690 hPa). The

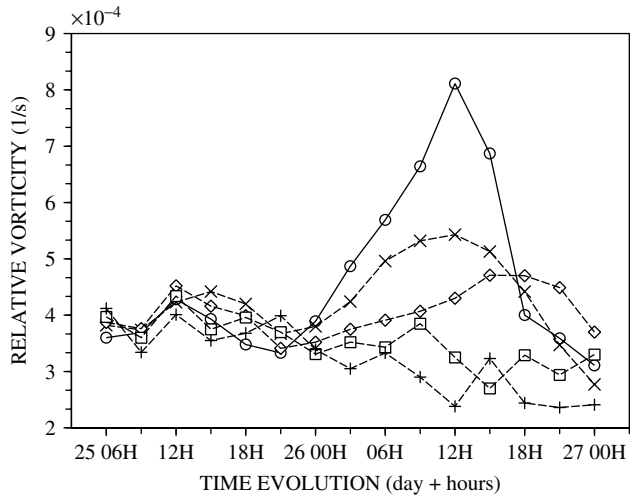

Figure 11. Time evolution of the vorticity maximum at 850 hPa for the control run (solid black line with ○), and when removing from the initial conditions all the high-frequency upper-level anomalies of the operational analysis and 25% (dashed line with ×), 50% (dashed line with ◇), 75% (dashed line with □) and 100% (dashed line with +) of the amplitude of the low-frequency anomaly in the whole troposphere (i.e. the low-frequency PV anomaly between 10 and 850 hPa and the low-frequency temperature anomaly at 850 hPa).

low-frequency amplitude parameters $A_{\rm lf} = B_{\rm lf}$ are set to 0.25, 0.5, 0.75 and 1.0 between 10 and 850 hPa. As more of the low-frequency anomalies amplitude is removed, the intensity of the storm decreases and its growth stage tends to vanish. For both cases $A_{\rm lf}$ =0.25 and 0.5, the growth is still present but weaker than in the cases in Figure 10. Note that for $A_{\rm lf}$ =0.5, the growth is delayed because of a global decrease of the westerlies that advect the surface cyclone less rapidly. For $A_{\rm lf}$=0.75 and 1.0, the growth stage disappears. This leads to the conclusion that there exists a threshold from which the low-level cyclone is not able to interact constructively with the upper-level jet stream. As shown in Figure 12(b), zonal winds reach 50 m s^{-1} in the upper troposphere for $A_{\rm lf}$=0.75. This is not a small speed yet the remaining baroclinicity seems not large enough to produce the intensification stage.

5.2. *Low-frequency disturbances at the lower boundary*

In the previous section the whole troposphere was modified, while in the present case only the low-frequency anomaly at the lower boundary (i.e. the temperature at 850 hPa) is partly removed ($A_{\rm hf} = A_{\rm lf} = B_{\rm hf} = 0$, $B_{\rm lf} \neq 0$). Increasing $B_{\rm lf}$ reduces the low-level baroclinicity. The suppression of the temperature anomaly shown in Figure 13(b) for $B_{\rm lf} = 1.0$ results in a strong decrease of the low-level temperature gradient in the modified flow (Figure 13(d)). This implies an increase of the zonal winds because the suppression of a warm and of a cold anomaly to the south and north of T1 leads at these levels to the suppression of cyclonic and an anticyclonic circulation respectively. Hence, this modification tends to increase the westerlies in the low levels (compare Figures 13(c) and (d)) making the eastward translation of the surface cyclone faster. This is the reason why the explosive growth stage for $B_{\rm lf} = 0.25$, 0.5 and 0.75 occurs sooner than in CTRL, but it is also weaker in terms of the relative vorticity maximum reached by the surface cyclone (Figure 14). It is interesting to note the abrupt transition from $B_{\rm lf} = 0.75$ to 1.0 for which the growth disappears suddenly (line with + in Figure 14). Complementary numerical experiments (not shown here) have been performed by removing only the low-frequency PV anomalies in the upper troposphere without any modification of the boundary condition. Although this leads to a continuous decrease of the growth stage, it was found difficult to suppress the storm as completely as with $B_{\rm lf} = 1.0$. To conclude, the low-level baroclinicity is one of the key parameters maintaining the amplitude of the surface cyclone and its subsequent rapid intensification stage.

5.3. *Displacement of the low-frequency jet exit*

RJ06 have explained the location of the explosive growth stage far downstream of the maximum baroclinicity in the jet-exit region by the three-dimensional structure of the large-scale environment. The eastward translation of the low-level cyclone is closely linked to the advection by the low-level jet that converges toward the upper-level jet in its exit region only. This can be understood from semi-geostrophic arguments; as the zonal wind speeds

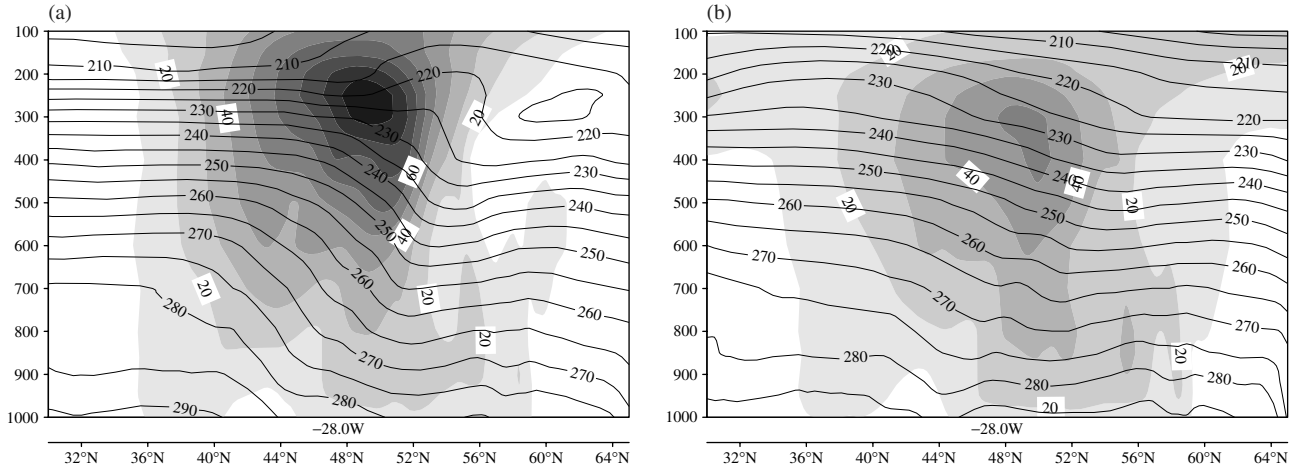

Figure 12. Vertical cross-sections at 28° W of the zonal wind (shading with interval 10 m s^{-1}) and the temperature (contours with interval 5 K) for (a) the control run and (b) the run with 75% reduction of the low-frequency anomalies.

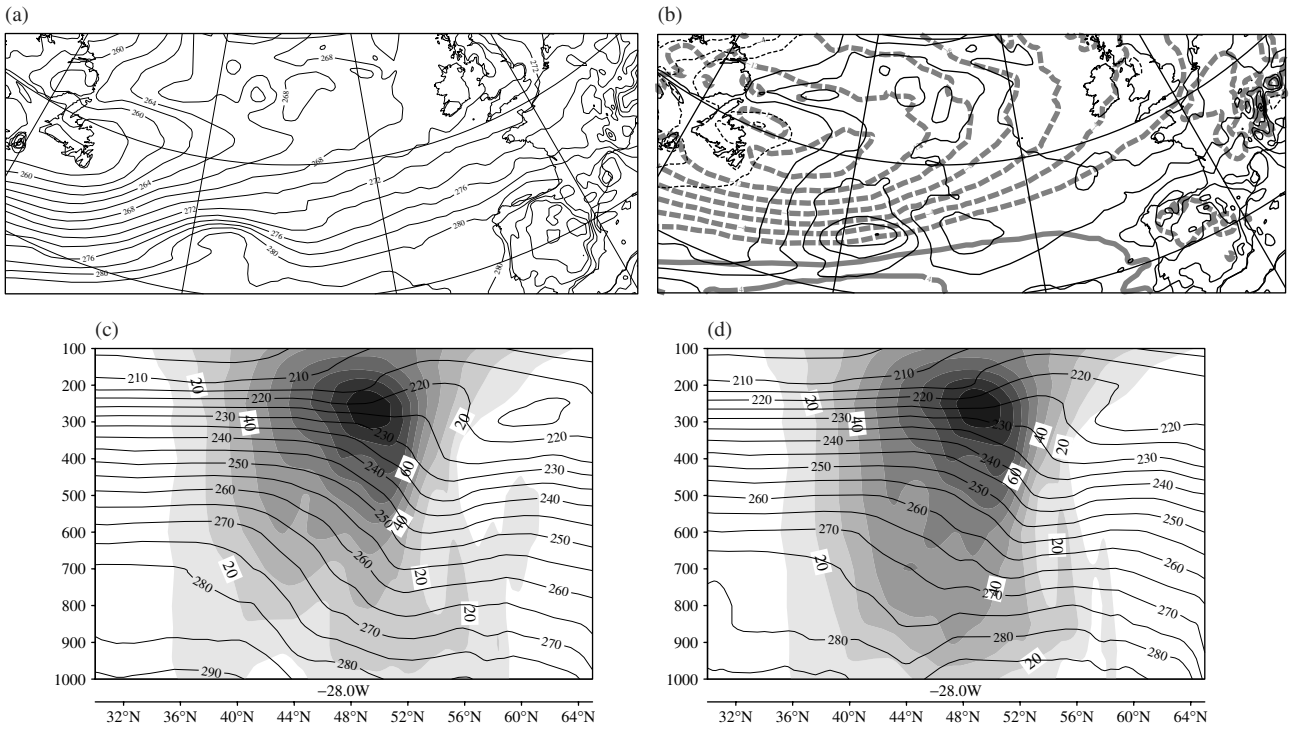

Figure 13. Temperature at 850 hPa at the initial time for (a) the control run and (b) the run where 100% of the low-frequency part has been removed (solid contours with interval 2 K). In (b), grey contours show the temperature anomaly relative to the control run (dashed and solid lines for negative and positive values, respectively, with interval 2 K). Also shown are vertical cross-sections at 28° W of the zonal wind (shading with interval 10 m s^{-1}) and temperature (black contours with interval 5 K) for (c) the control run and (d) the run without the low-frequency part.

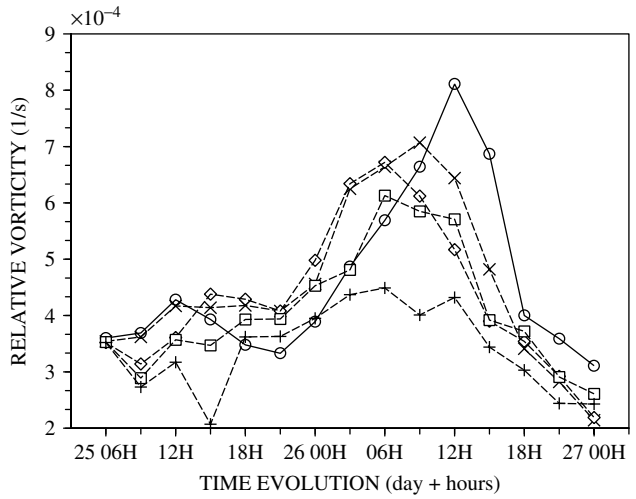

Figure 14. Time evolution of the vorticity maximum at 850 hPa for the control run (solid line with ○), and the runs made by removing initially 25% (line with ×), 50% (line with ◇), 75% (line with □) and 100% (line with +) of the low-frequency temperature anomaly at 850 hPa.

of the jets decrease, their meridional relative distance decrease as well. The jet-exit region seems therefore to be a preferential region where surface cyclones will reach the location of the upper-level jet axis and rapidly intensify.

To check the importance of the jet exit, two runs differing in the position of the jet exit are compared in Figures 15–17. The non-modified jet exit consists of removing all the high-frequency anomalies in the upper levels and keeping the low-frequency ones as they are in CTRL. The jet-exit region is thus the same as in CTRL and is located to the east of 20° W (Figure 15(a)). To displace the jet-exit region more upstream, low-frequency anomalies in the whole troposphere have been removed from a wide longitude band in the eastern Atlantic leading to the flow shown in Figure 15(b). The maximum of the upper-level zonal wind is reached at 50° W, more upstream than that of the non-modified jet-exit case also with a slightly weaker value (around 75 m s^{-1}). The decrease of the westerlies are already visible east of that longitude. The jet-exit region is thus located more upstream in Figure 15(b) than in (a). Because of this rapid deceleration in the modified jet-exit case, the low-level zonal winds are vertically aligned with the upper ones at 30° W (Figure 15(d)). In contrast, at the same longitude, the zonal winds in the non-modified jet-exit case exhibit a clear northward tilt with height (Figure 15(c)). Because of these dynamical differences, we expect a crossing of the upper-level jet axis by the surface cyclone sooner in the modified jet-exit run.

In the modified jet-exit run, the surface cyclone (diamonds in Figure 15(b)) indeed does move to the north more rapidly than in the non-modified case (Figure 15(a)), especially during the first 12 h. This difference in the trajectory is also visible by comparing Figures 16(c) and (d). A change in the shape of the surface cyclone, which is less zonally stretched in the modified jet-exit case, can be also noticed. The surface cyclone crosses the upper-level jet more upstream at 20° W while the corresponding longitude is around 10° W in the non-modified jet-exit case. Figure 17 shows that the timing of the explosive growth stage is roughly the same with a weaker growth for the more upstream jet exit because of the reduction of the baroclinicity throughout

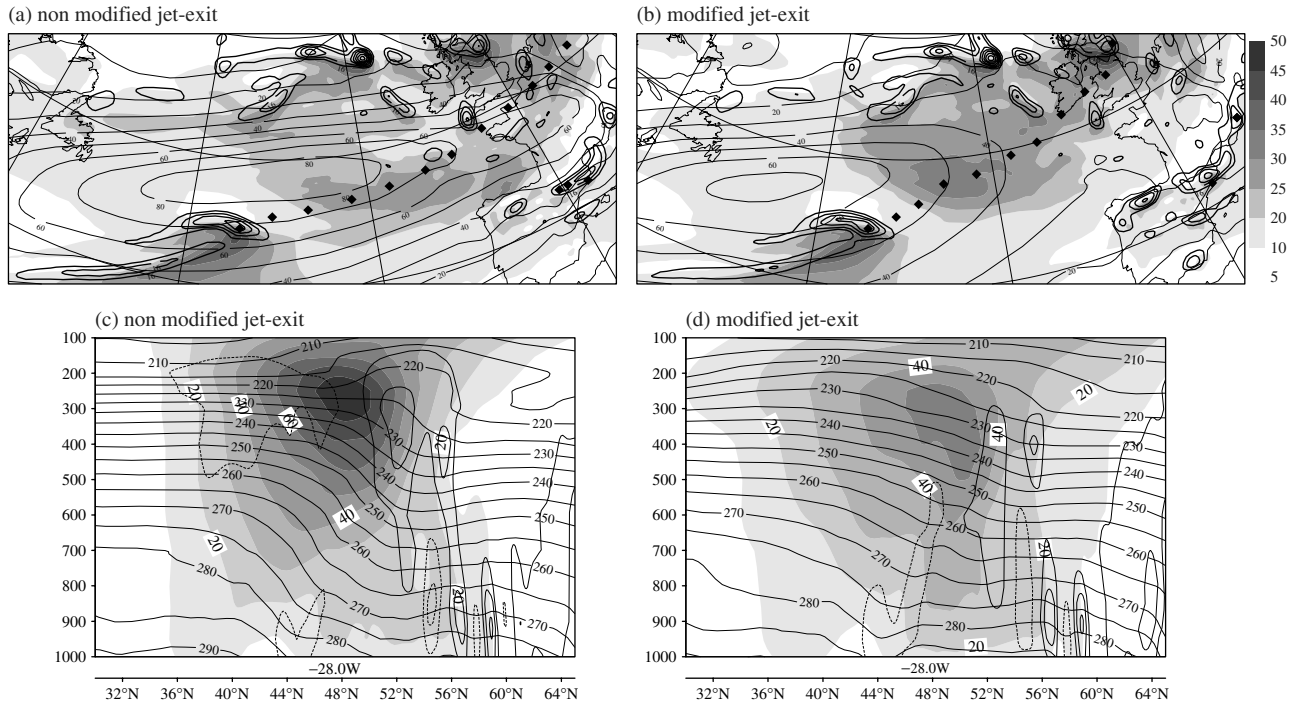

Figure 15. Trajectory of the maximum vorticity at 850 hPa (black ◇) for the run without upper disturbances with (a) an unmodified and (b) a modified jet exit. The zonal wind at 850 hPa (shading with interval 5 m s^{-1}) and at 300 hPa (thin black contours with interval 10 m s^{-1}) and the relative vorticity at 850 hPa (bold black contours with interval 8×10^{-5} s^{-1}) are added at the initial time. (c) and (d) show vertical cross-sections at 28° W of the zonal wind (shading with interval 10 m s^{-1}), the temperature (black thin contours with interval 5 K) and the relative vorticity (dashed and solid contours for negative and positive values, respectively, with interval 5×10^{-5} s^{-1}) for the runs with (c) an unmodified and (d) a modified jet exit.

its trajectory. The difference between the two runs lies in the fact that the growth rate location is not the same. After 18 h (0000 UTC, 26 December), the cyclones in both runs start their intensification stage but for the modified jet exit it is located at 14° W, 50° N while it is at 9.5° W, 48° N for the other case.

In conclusion, these results support the idea that the large-scale zonal winds in the low levels determine to a large extent the trajectory of the surface cyclone. The jet-exit region is a preferential region for the interaction of a surface cyclone with the upper-level jet due to the vertical alignment of the large-scale winds in this area. We have checked that the modified jet-exit run is the one exhibiting the strongest difference from the CTRL surface cyclone trajectory of all the runs shown in the present paper. This experiment validates some of the important conclusions of RJ06.

6. The role of the shape and location of idealized low-level cyclones

As shown in section 4.1, high-frequency upper-level disturbances have a moderate impact on the development of T1 while the results of Hello and Arbogast (2004) on T2 have revealed a strong sensitivity of the storm to upper-level disturbances. It has been checked (not shown here) that indeed the removal of the high-frequency disturbances leads to the complete and rapid suppression of the T2 storm when it is located at approximately the same place as T1 at 0600 UTC on 25 December. What are the essential ingredients that make the interaction with the upper-level jet happen for T1 and not for T2 while they evolve in roughly the same large-scale environment? Few differences are visible in the structure and position of the two surface cyclones before reaching the upper-level jet. T2 has a much more zonally stretched structure (RJ06) than T1 and its trajectory was 1 or 2° more to the south. To look at the sensitivity to the shape and location of the surface cyclones, idealized ones have been constructed with a Gaussian shape having different position and aspect ratio. The process is as follows: the low-level cyclone T1 is first removed at 0600 UTC on 25 December and then replaced by an idealized one having the same maximum amplitude in PV (between 520 and 850 hPa) and temperature at 850 hPa.

The evolutions of two of these idealized surface cyclones centred at the same location as T1 at 0600 UTC on 25 December (i.e. at 36° W, 45° N) are compared in Figure 18. In Figure 18(a) the initial surface cyclone is weakly stretched zonally similar to T1, while in Figure 18(b) it is strongly stretched as T2. The impact on their respective evolution is already visible after 12 h (Figures 18(c),(d)). The relative vorticity amplitude of the strongly stretched perturbation (Figure 18(d)) has decreased rapidly whereas that of the weakly stretched perturbation maintains itself (Figure 18(c)). The latter is slightly more to the north than the former with a clearer interaction with upper levels and a much greater vertical velocity. An explosive growth stage occurs for the weakly stretched perturbation with more or less the same timing as in CTRL (asterisks in Figure 19(a)), while for the strongly stretched case there is only a weak growth at the jet exit (asterisks in Figure 19(b)).

The influence of the latitudinal position of the idealized surface cyclones is shown in Figure 19. For a more northward position (at 46.5° N) an explosive growth stage happens for both the weakly and strongly stretched perturbations (curves

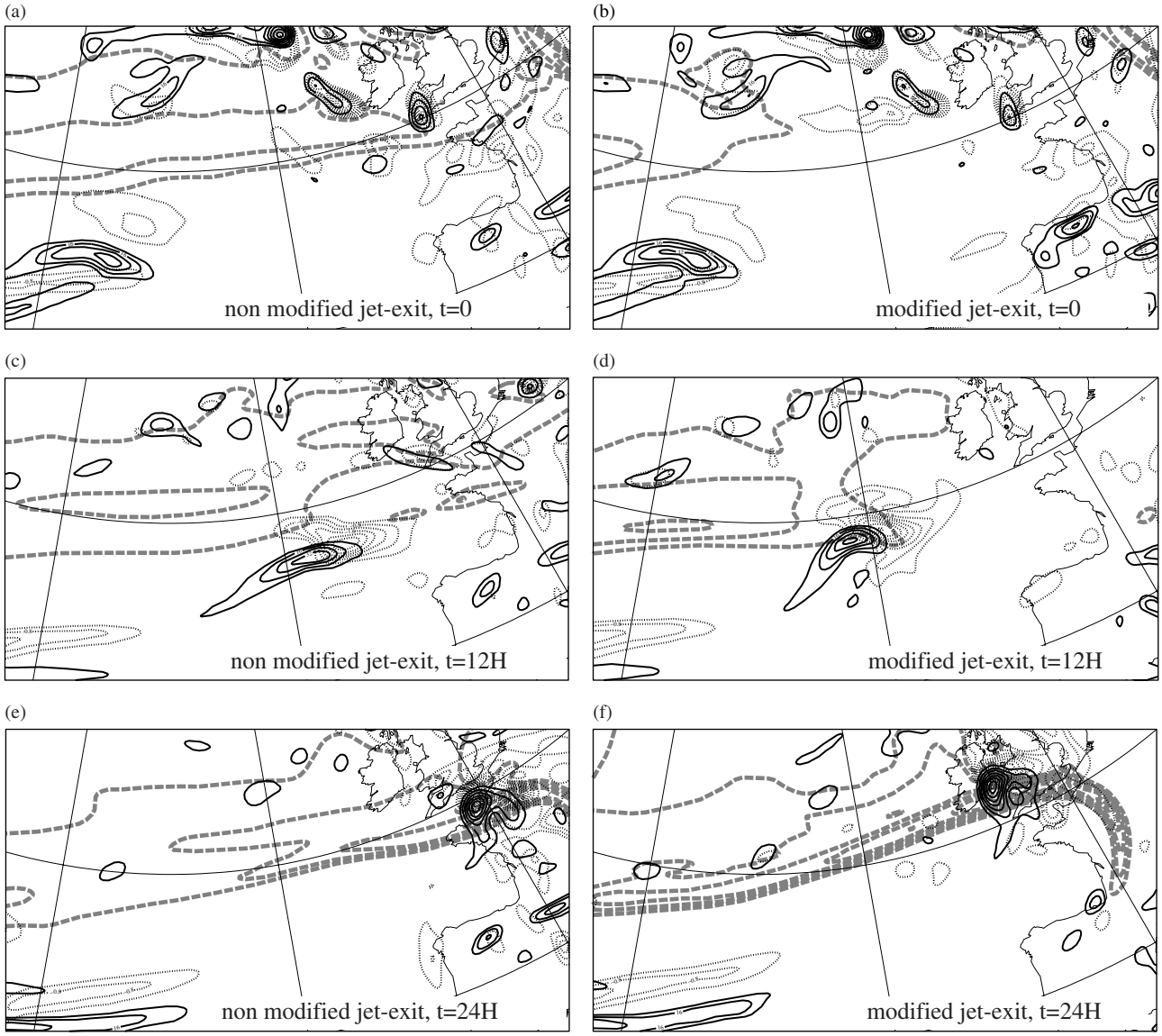

Figure 16. As Figure 2, but for the run (a, c, e) without modification of the jet exit and (b, d, f) with a modified jet exit.

with $\triangle$), while for a more southward position (at 43.5° N) no significant growth appears, whatever stretching is applied (curves with $\triangledown$).

To summarize, a strong sensitivity to the shape and the latitudinal position of the surface cyclones is found. The closer the initial position of the surface cyclone to the upper-level jet, the stronger is its explosive growth stage. This rapid intensification stage can even disappear entirely with a slight initial southward displacement of the surface cyclone (e.g. 1.5° latitude). Concerning the influence of the initial shape, a more isotropic and confined low-level structure seems to be more able to propagate rapidly poleward and to interact with the upper-level jet than a stretched surface cyclone. This provides a rationale for the need for T2 (unlike T1) to have an upper-level precursor in order to grow rapidly.

7. Concluding remarks

Numerical sensitivity experiments have been systematically performed to reveal a number of key dynamical ingredients leading to the explosive growth stage of the European wind storm *Lothar* (Table I gives a summary). A new look at the

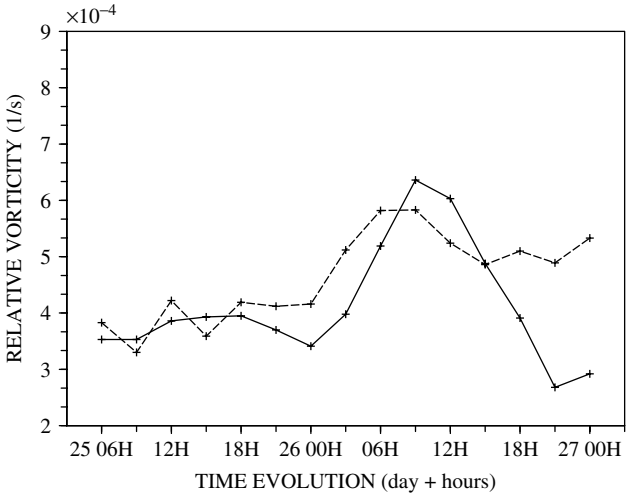

Figure 17. Time evolution of the vorticity maximum at 850 hPa for the runs with an unmodified jet exit (solid line with +) and a modified jet exit (dashed line with +).

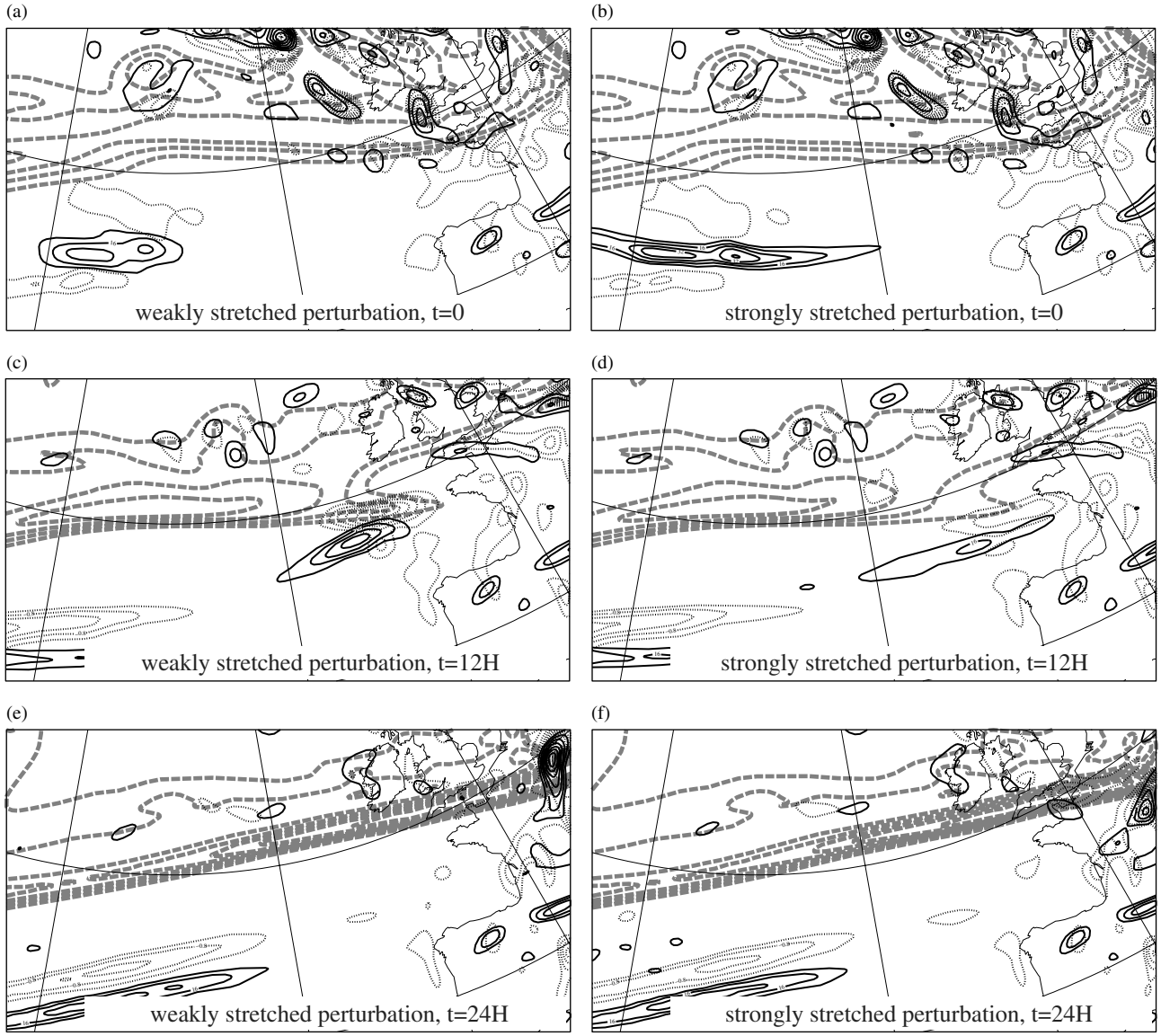

Figure 18. As Figure 2, but for the run (a, c, e) with a weakly stretched low-level perturbation and (b, d, f) with a strongly stretched perturbation.

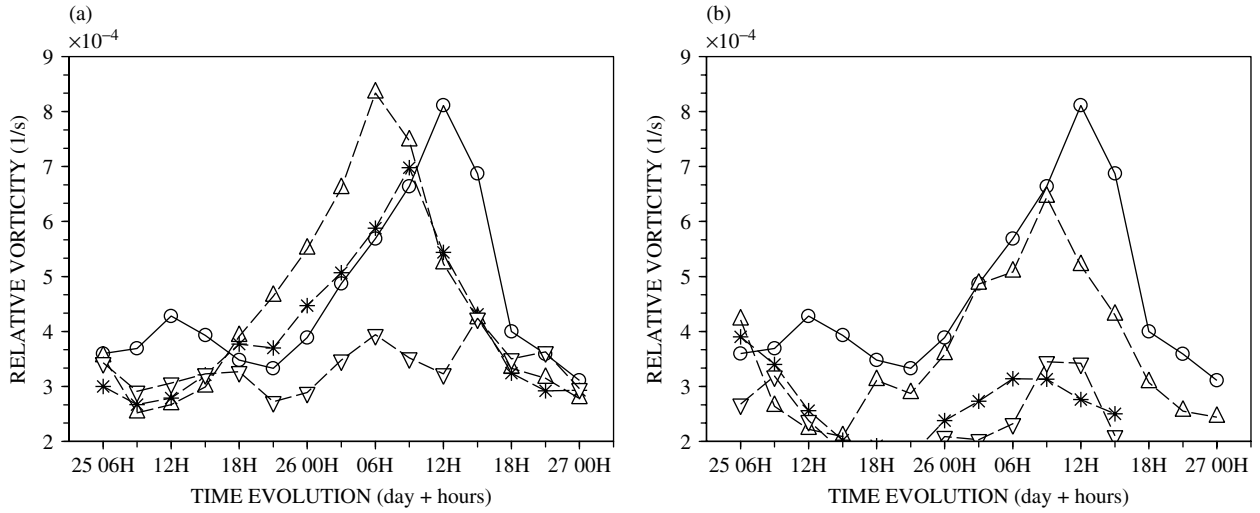

Figure 19. Time evolution of the vorticity maximum at 850 hPa for an initial perturbation located at 36° W and 46.5° N (line with △), 45° N (line with ∗) and 43.5° N (line with ▽) for (a) a weakly stretched and (b) a strongly stretched perturbation.

Table I. Summary of the different numerical sensitivity experiments. More details are given in the text.

Section in text	Experiment description	Definition of the anomalies				Vorticity amplification /phase duration (h)	Vorticity maximum (10^{-4} s^{-1})	Main result
		A_{hf} (levels)	A_{lf} (levels)	B_{hf}	B_{lf}			
2	Control (CTRL)	–	–	–	–	2.4/15	8.1	Storm[a]
3	No humidity	–	–	–	–	–	–	No growth[c]
	Adiabatic run	–	–	–	–	2.2/15	8.7	Storm
4.1	Reduction of surface cyclone amplitude	0.25(L)	0	0.25	0	2.2/15	6.8	Storm
		0.5 (L)	0	0.5	0	1.5/ 6	4.0	Weak low[b]
4.2	No monopole	1.0 (U)	0	0	0	2.2/15	7.8	Storm
	No dipole	1.0 (U)	0	0	0	1.9/ 9	6.7	Storm
	No upper disturbances	1.0 (U)	0	0	0	1.9/ 9	6.4	Storm
5.1	Sensitivity to low-frequency disturbances in the whole troposphere	1.0 (U)	0.25(T)	0	0.25	1.5/15	5.4	Weak low
		1.0 (U)	0.5 (T)	0	0.5	1.4/18	4.7	Weak low
		1.0 (U)	0.75(T)	0	0.75	–	–	No growth
		1.0 (U)	1.0 (T)	0	1.0	–	–	No growth
5.2	Sensitivity to low-frequency disturbances at the lower boundary	0	0	0	0.25	1.7/12	7.1	Storm
		0	0	0	0.5	1.6/ 9	6.7	Storm
		0	0	0	0.75	1.5/ 9	6.1	Storm
		0	0	0	1.0	–	–	No growth
5.3	Non-modified jet exit	1.0 (U)	0	0	0	1.9/ 9	6.4	Traj. as CTRL
	Modified jet exit	1.0 (U)	1.0 (T)	0	1.0	1.4/ 9	5.8	Modified traj.
6	Weakly stretched (46.5° N)	1.0 (L)	0	1.0	0	3.3/21	8.3	Storm
	(45° N)	1.0 (L)	0	1.0	0	1.9/12	7.0	Storm
	(43.5° N)	1.0 (L)	0	1.0	0	–	–	No growth
	Strongly stretched (46.5° N)	1.0 (L)	0	1.0	0	2.2/12	6.4	Storm
	(45° N)	1.0 (L)	0	1.0	0	–	–	No growth
	(43.5° N)	1.0 (L)	0	1.0	0	–	–	No growth

[a] a cyclone having at least three quarters the maximum amplitude of CTRL.
[b] a cyclone not reaching this amplitude, but presenting significant growth.
[c] no significant deepening from the initial amplitude.
L = 520–850 hPa; U = 10–690 hPa; T = 10–850 hPa.

role played by the physical processes has first shown that a frictionless dry adiabatic run is able to reproduce the timing and the location of the rapid intensification stage while its intensity becomes overestimated. W02 have proposed the 'bottom-up development' concept to characterize the rapid intensification stage of T1. Namely, a low-level cyclone interacting with an upper-level jet creates a tropopause fold just upstream of it during its crossing of the jet. This then reinforces the baroclinic interaction and the deepening of the surface cyclone. Their study has emphasized the crucial role played by moist processes during this phase. In the present study, moist processes were found to be crucial in the sense that they correspond to a source term that compensates for the dissipative effects. However, the vertical coupling between the surface cyclone and the upper-level jet (i.e. the 'bottom-up development') can be reproduced and interpreted entirely in terms of dry adiabatic interactions, at least for conceptual purposes. This result is important because it allows the possibility of reproducing the behaviour of T1 in future studies within the idealized framework of simple dry models such as, for example, semi-geostrophic dry models.

The second goal of our study was to investigate the possible influence of high-frequency disturbances in the upper troposphere prior to the explosive growth stage. A dipole anomaly in the high-frequency PV field was detected

at least 12 h before the rapid intensification stage suggesting that an interaction with the upper-level jet stream at that time has already begun while the surface cyclone is far south of this jet. In other words, this dipole is not an independent structure but one that the surface cyclone itself and the jet are creating by interacting with one another. The removal of this dipole anomaly has a moderate impact resulting in a 25% reduction of the storm intensity. This dipole is rapidly regenerated when the surface cyclone approaches the upper-level jet axis and its pre-existence 12 h before the start of the explosive growth stage cannot therefore be considered as a triggering ingredient.

After removing all the high-frequency upper-level anomalies, two essential elements still remain in the flow: the surface cyclone itself and the low-frequency flow characterized by strong baroclinicity and exceptional wind speeds in the upper troposphere (more than $80\,\mathrm{m\,s^{-1}}$). As expected, by systematically decreasing the intensity of the low-frequency anomalies (i.e. by decreasing both the baroclinicity and the strength of the upper-level jet) the intensity reached by the storm decreases and a threshold exists from which its growth phase disappears. It is curious to note that this suppression happens while the upper-level jet keeps speed values close to the climatology. The low-level baroclinicity was found to be a more important parameter for the growth rate of the storm than the low-frequency PV anomalies in the upper troposphere.

Another set of experiments has examined the role played by the position of the jet exit in the location of the explosive growth stage, confirming the results of RJ06. When the jet exit is displaced more upstream, it tends to place more upstream the vertical alignment of the low-level zonal winds with the upper ones. The consequence is that the low-level cyclone, whose trajectory is constrained by the low-level zonal winds, will cross the upper-level jet axis more upstream too. However, the jet-exit region generally covers a large area and it was found difficult to get a better diagnostic to localize *a priori* the crossing of the jet by the surface cyclone. In RJ06, the authors have shown that a more precise diagnostic is based on the deformation field of the two low-frequency jets and on the effective deformation introduced in their study. But the low-frequency field is not defined once the flow is abruptly changed at the initial time. A full 'low-frequency' history leading to the modified flow would be needed to achieve this. A sign of this difficulty is that the effective deformation field was found too noisy when computed from the total flow. Future studies will investigate this aspect.

Different experiments have shown that the amplitude, the shape and the location of the surface cyclone relative to the upper-level jet are crucial parameters for its explosive growth stage. A stronger amplitude at the initial time eases the later interaction with the upper-level jet and so does a closer position to the latter jet. Furthermore, a more confined and less stretched structure of the surface cyclone is a more favorable situation. An important concluding remark from all the numerical experiments is the strong sensitivity of the explosive growth stage to the low-level features of the initial flow and especially to the surface cyclone itself. By changing its position only slightly, a drastic change in its evolution may happen. Also less sensitivity to upper-level dynamical features was detected globally. This conclusion should be kept in mind when thinking of improvements to the forecasting of such extreme events.

Finally, future studies should investigate more carefully the crossing of a large-scale jet by a surface cyclone. The explosive growth stage that occurs during the crossing in its left-exit region is usually related to the mechanism proposed by Uccellini (1990). In the latter study, the reasoning is based on an upper-level jet streak and it is not obvious that the result can be extended to a low-frequency jet stream. Nowadays, alternatives become available. One is the concept of 'bottom-up development' presented in W02 and extended in the present study. Another stems from the recent work from Gilet *et al.* (2009) showing a cyclone deepening as it crosses a pure zonal jet (i.e. without the presence of any diffluence). Both suggest the existence of other mechanisms explaining the growth of a surface cyclone as it crosses an upper-level jet axis.

Acknowledgements

Fabien Crépin is sincerely acknowledged for his preliminary results obtained a few years ago which constituted the start of our study. We thank also the two reviewers for their suggestions which significantly improved the paper. GR acknowledges the support of ANR through contract ANR-06-JCJC-0133.

References

Arbogast P, Maynard K, Crépin F. 2008. Ertel potential vorticity inversion using a digital filter initialization method. *Q. J. R. Meteorol. Soc.* **134**: 1287–1296.

Bougeault P. 1985. A simple parameterization of the large-scale effects of cumulus convection. *Mon. Weather Rev.* **113**: 2108–2121.

Courtier P, Freydier C, Geleyn J-F, Rabier F, Rochas M. 1991. 'The ARPEGE project at Météo-France'. In *Proceedings of seminar on numerical methods in atmospheric models*. 9–13 September 1991. ECMWF: Reading, UK. 193–231.

Descamps L, Ricard D, Joly A, Arbogast P. 2007. Is a real cyclogenesis case explained by generalized linear baroclinic instability? *J. Atmos. Sci.* **64**: 4287–4308.

Gilet J-B, Plu M, Rivière G. 2009. Nonlinear baroclinic dynamics of surface cyclones crossing a zonal jet. *J. Atmos. Sci.* **66**: 3021–3041.

Hello G, Arbogast P. 2004. Two different methods to correct the initial conditions applied to the storm of 27 December 1999 over southern France. *Meteorol. Appl.* **11**: 41–57.

Lopez P. 2002. Implementation and validation of a new prognostic large-scale cloud and precipitation scheme for climate and data-assimilation purposes. *Q. J. R. Meteorol. Soc.* **128**: 229–257.

Morcrette J-J, Mlawer EJ, Iacono MJ, Cough SA. 2001. 'Impact of the radiation transfer scheme RRTM in the ECMWF forecasting system'. *ECMWF Newsletter* **91**: 2–9.

Noilhan J, Planton S. 1989. A simple parameterization of land surface processes for meteorological models. *Mon. Weather Rev.* **117**: 536–549.

Parker DJ, Thorpe AJ. 1995. Conditional convective heating in a baroclinic atmosphere: A model of convective frontogenesis. *J. Atmos. Sci.* **52**: 1699–1711.

Petterssen S, Smebye SJ. 1971. On the development of extratropical cyclones. *Q. J. R. Meteorol. Soc.* **97**: 457–482.

Rivière G, Joly A. 2006. Role of the low-frequency deformation field on the explosive growth of extropical cyclones at the jet exit. Part II: Baroclinic critical region. *J. Atmos. Sci.* **63**: 1982–1995.

Røsting B, Kristjánsson JE. 2006. Improving simulations of severe winter storms by initial modification of potential vorticity in sensitive regions. *Q. J. R. Meteorol. Soc.* **132**: 2625–2652.

Ulbrich U, Fink AH, Klawa M, Pinto JG. 2001. Three extreme storms over Europe in December 1999. *Weather* **56**: 70–80.

Uccellini LW. 1990. Processes contributing to the rapid development of extratropical cyclones. In *Extratropical Cyclones: The Erik Palmén Memorial Volume*. Newton C, Holopainen EO (eds.) Amer. Meteorol. Soc: Boston, USA. 81–105.

Wernli H, Dirren S, Liniger MA, Zillig M. 2002. Dynamical aspects of the life cycle of the winter storm *Lothar* (24–26 December 1999). *Q. J. R. Meteorol. Soc.* **128**: 405–429.